Coatings **2015**, *5*, 78-94; doi:10.3390/coatings5010078

OPEN ACCESS

coatings

ISSN 2079-6412

www.mdpi.com/journal/coatings

Article

Study on the Correlation between Microstructure Corrosion and Wear Resistance of Ag-Cu-Ge Alloys

Antonio Cusma [1,*], Marco Sebastiani [2], Daniele De Felicis [2], Andrea Basso [3] and Edoardo Bemporad [2]

[1] Department of Chemistry and Materials Science, National Research Council of Italy, Via dei Taurini 19, Rome 00185, Italy

[2] Engineering Department, "Roma TRE" University, Via della Vasca Navale 79, Rome 00146, Italy; E-Mails: marco.sebastiani@uniroma3.it (M.S.); daniele.defelicis@uniroma3.it (D.D.F.); edoardo.bemporad@uniroma3.it (E.B.)

[3] Legor Group SRL, Via San Benedetto14-34, Bressanvido, VI 36050, Italy; E-Mail: andrea_b@legor.com

* Author to whom correspondence should be addressed; E-Mail: antonio.cusma@cnr.it; Tel.: +39-06-4993-2317.

Academic Editor: Alessandro Lavacchi

Received: 23 December 2014 / Accepted: 9 March 2015 / Published: 13 March 2015

Abstract: In this work, a morphological and structural characterization of a ternary Ag-Cu-Ge alloy of known composition was performed with the aim of evaluating how the passivation parameters (time and temperature) influence the morphological features of the material surface. A nanomechanical characterization was performed in order to correlate the morphology and microstructure of the alloy with its tarnish, wear, and scratch resistance. It was found that the addition of germanium to the alloy not only provides the material with tarnish and fire-stain resistance, but it also improves the scratch and wear resistance owing to the formation of a dense and stable thin oxide layer.

Keywords: silver alloy; germanium; SEM; TEM; passivation; thin films

1. Introduction

Ternary Ag-Cu-Ge alloys are materials that have two main fields of application. An alloy consisting of at least 77 wt% silver, between 0.4% and 7% germanium and the remainder being copper has been proposed as a material for joining two elements in welding or brazing, since it reduces the problems connected with fire stain that arise whenever copper oxidizes at high temperatures [1].

Furthermore, such alloys are widely used in the manufacture of jewels and silverware, since the addition of a small quantity of germanium to the alloy commonly known as Sterling is known to reduce the issues related to tarnishing and fire stain that affect common silver alloys [2,3].

Sterling silver is one of the most widely used silver alloys to produce fine jewellery. The international standard has fixed a minimum of 92.5 wt% [4] of silver in the alloy, but no limitations have been issued about the other constituents [5]. However, since the fourteenth century, silversmiths have used copper for the remaining 7.5% since Cu improves the hardness and strength of the soft silver. Modern manufacturers also add a small quantity of other elements such as cadmium (to improve ductility) and boron (as a grain refiner) [3]. The microstructure of this kind of alloy usually consists of two main phases, the first one (matrix) rich in silver, the second one rich in copper, which can also be eutectic, depending on composition.

The main issue with Sterling silver is that it is subject to tarnish and fire-stain which greatly affect the pure lustre of silver [5–9]. The addition of different metals in the alloy has been proposed to reduce tarnish and/or fire-stain. Aluminium can prevent tarnish by forming aluminium oxide (transparent), but it makes the alloy too hard for forming [6]; Zinc, cadmium, and silicon have all been used to improve the tarnish resistance properties of the alloy since they help by reducing the quantity of oxygen, but they also impoverish the strength of the material [7,8].

The addition of a certain quantity of germanium to Ag-Cu alloys is a known technique used to improve the tarnish and fire-stain resistance of the artefacts, to form an alloy commonly known as "Argentium" [10]. The presence of Ge induces—after an opportune passivation heat treatment—the formation of a thin, transparent germanium oxide layer that does not affect the aesthetic properties of the artefacts, providing in the meantime the protection of the bulk material from aggressive agents like sulphides [9].

Even though a lot of work has been carried out by many authors on pure Sterling silver, and in particular on its microstructure, precipitation kinetics and hardening mechanism [11–14], the study of Ag-Cu-Ge alloy structure and properties has not been much investigated. To the authors' understanding, there is still a significant gap of knowledge in the literature on the actual microstructural mechanisms that regulate the functional (*i.e.*, tarnish resistant) behavior of Ag-Cu-Ge alloys. In particular, three main critical issues have not been yet investigated in detail and require a deeper and more comprehensive analysis: (i) the influence of time and temperature on the oxide layer thickness and structure during the passivation heat treatment, (ii) the actual morphology, structure, composition and surface distribution of the oxide layer itself, (iii) the correlations (if any) between the thickness and microstructure of the oxide layer and the surface mechanical properties of the alloy, in terms of scratch resistance and friction during sliding contact.

In this work, we focus on the jewellery application and investigate the influence of heating parameters on the morphological and structural characteristics of Ag-Cu-Ge ternary alloy of known composition, as

well as the correlation between the morphological features of the alloy and its tarnish resistance properties. Specific focus is given to the analysis of the oxide layer thickness and structure as a function of temperature and time of passivation. Also the correlation between the passivation parameters and the mechanical properties of the alloy is investigated in order to achieve further information on how the surface characteristics affect the hardness and wear resistance of the alloy.

The samples were largely and extensively characterized from a morphological (SEM, TEM and AFM analysis), structural (XPS and EDS analysis), and micromechanical (nanoindentation and nanoscratching) point of view.

2. Experimental Section

Samples of Ag-Cu-Ge were provided by the manufacturer (Legor Group, Bressanvido, Italy) with the following composition: Ag 93.5 wt%, Cu 5.5 wt%, Ge 1 wt%. Four different set of samples were produced at different passivation temperatures and times. Samples were laminated and polished prior to heat treatment.

Sample 1467 did not undergo any heating treatment, while sample 1468 was prepared according to the most frequently used values for heating parameters (heated at 100 °C in air for 3 h). Sample 1469 was prepared in order to see if an increase of passivation time would produce better results, therefore, the passivation time was extended to 16 h, while keeping the temperature at 100 °C. Sample 1470, heated at 200 °C for 2 h, was prepared to evaluate if a higher temperature would result in a similar result to the standard sample but with a reduced time, thus increasing the production rate.

Microstructural and morphological analyses were performed by Field Emission Gun-SEM investigations, using a FEI Helios Nanolab 600 Dual Beam FIB/SEM equipment (FEI, Hillsboro, OR, USA).

Focused Ion Beam (FIB) techniques [15] were used for TEM lamella preparation. A finished electron transparent portion of the sample (usually 5 μm × 20 μm) was obtained by FIB micro-milling and then, via a micro-manipulator, placed on a sample holder and inserted into the TEM microscope. A thin platinum layer is usually deposited on the sample surface to protect its outer layer from ion damage during FIB milling and thinning. This procedure represents the one site-specific and artefact-less outstanding TEM sample preparation technique. In this case, a TEM lamella (thickness lower than 100 nm) was obtained in correspondence with a grain boundary for each sample, thus allowing the microstructure analysis of both phases, including structure and thickness of the surface oxide layer. TEM-EDS and SAED analysis were then performed with a Philips CM120 microscope (FEI, Hillsboro, OR, USA).

SAED (Selected Area Electron Diffraction) is a crystallographic technique that uses the diffraction of the TEM electron beam with the atoms of the specimen in order to acquire an image consisting of a series of spots or rings pattern which recall the lattice structure. So the diffraction pattern is a series of spots in the case of a crystal, a series of rings in the case of a poly-crystal, while no spots or rings appear for an amorphous material. Even though SAED analysis could have provided information on the phases and materials present in the sample, in this case the thickness of the film was too small to allow an effective tilting of the sample without exiting the selected region of interest. However, SAED is a powerful technique to gain information on whether the material is crystalline or amorphous.

An NT-MDT SMENA (NT-MDT, Moscow, Russia) atomic force microscope was used for AFM measurements. It was chosen to work in semi-contact mode, in order to reduce the risk of anelastic deformation of the sample surface. Standard silicon tips and cantilevers were used.

XPS measurements were carried out to measure photoemission spectra of the core C1s, O1s, Ag3d, Cu2p and Ge3d, working with a Mg kα source, pass energy 25 eV, step 0.1 eV. Quantitative analysis referred to the values of binding energy reported in the NIST Standard Reference Database 20, Version 3.5.

The surface hardness and elastic modulus of the samples were investigated by nanoindentation [16,17] on the as received samples with a Nano Indenter G200 (Agilent Technologies, Santa Clara, CA, USA), equipped with a Berkovich indenter calibrated on a certified fused silica reference sample. Indentations were performed in a continuous stiffness measurement (CSM) mode, under a constant strain rate of 0.05 s^{-1}. A maximum penetration depth of 500 nm was set for all tests. A regular matrix of 16 indentations was performed on the primary phase with a spacing of 10 μm. Ten more indentations were performed on the grains of the secondary phase, after microscope use to indenter calibration of the instrument. In this way, the hardness and modulus *vs.* depth profiles were obtained for both the main phases of each sample. Nanoscratching [18] was performed with the same instrument, loading the sample up to a maximum of 0.5 mN (other test parameters: scratch length 200 μm, scratch velocity 1 μm/s). The friction coefficient was continuously monitored during the nanoscratch test.

To perform the tarnish test, samples were put in a test chamber and exposed to thioacetamide powder crystals (TAA) at 20 °C for 16 h for a standard TAA corrosion test, according to the ISO 4538 [19]. Then a colorimetric test was carried out in order to evaluate the changes in the colour coordinates before and after the corrosion test. Colorimetric analysis was performed using a GretagMacbeth Color i7 spectrophotometer (X-rite, Munich, Germany) and the result were referred to the CIELAB color coordinates [20].

3. Results and Discussion

3.1. Morphological and Microstructural Characterization

In Figure 1, SEM micrographs for the samples 1467 and 1469 are reported, showing that the samples have the typical two-phase structure, with a matrix—were Ag is predominant—and clusters of a second phase, rich in copper. Such morphology suggests that a slow, equilibrium cooling occurred [21,22].

Similar microstructures were evidenced for all the samples.

EDS cross-section profiles on TEM lamellae for the 1469 sample are shown in Figure 2. The profiles were performed for both the main phases. At least eight measurement points were performed for each analysis and the points were aligned on a path starting from about 100 nm deep into the surface of the samples and moving towards the platinum protective layers. The red arrows in Figure 3 show the points (approximately) and the direction of measurements. As shown in Figure 2 the matrix phase (α-phase) is mainly constituted of Ag, with a small amount of Cu and Ge, while it is in the β-phase, richer in copper, that most of the Germanium is alloyed. It is also in this phase that most of the oxide forms. However, even if some oxide forms in the α-phase, it is still Cu and Ge oxide, since the XPS showed that no Ag is present in its oxidized state. Similar trends were obtained for all the samples, and are not shown here for brevity.

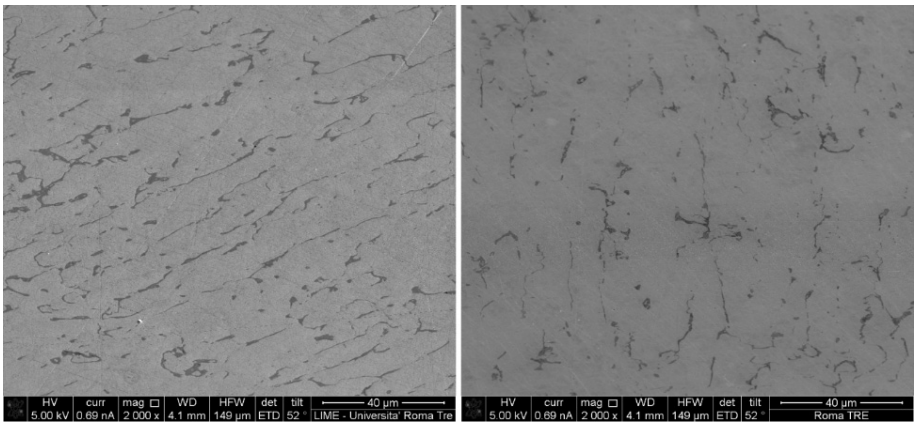

(**a**) (**b**)

Figure 1. SEM micrographs of samples (**a**) 1467 and (**b**) 1469.

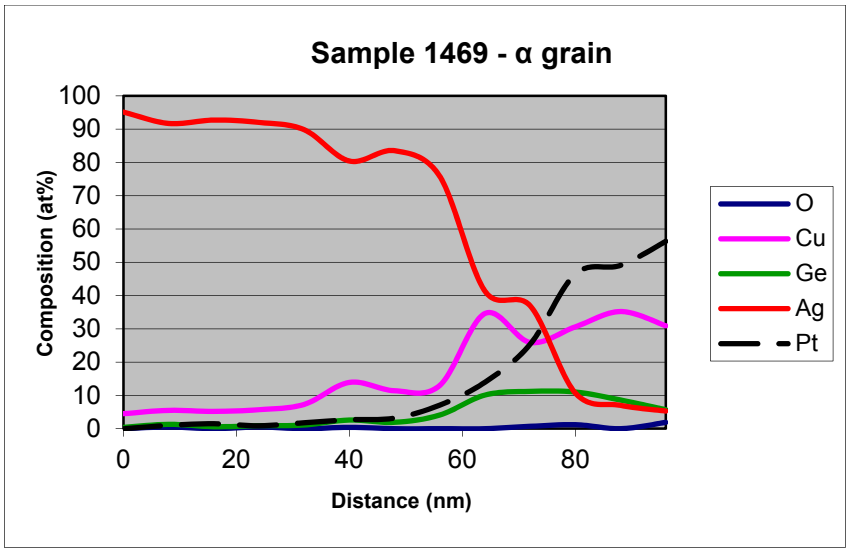

(**a**)

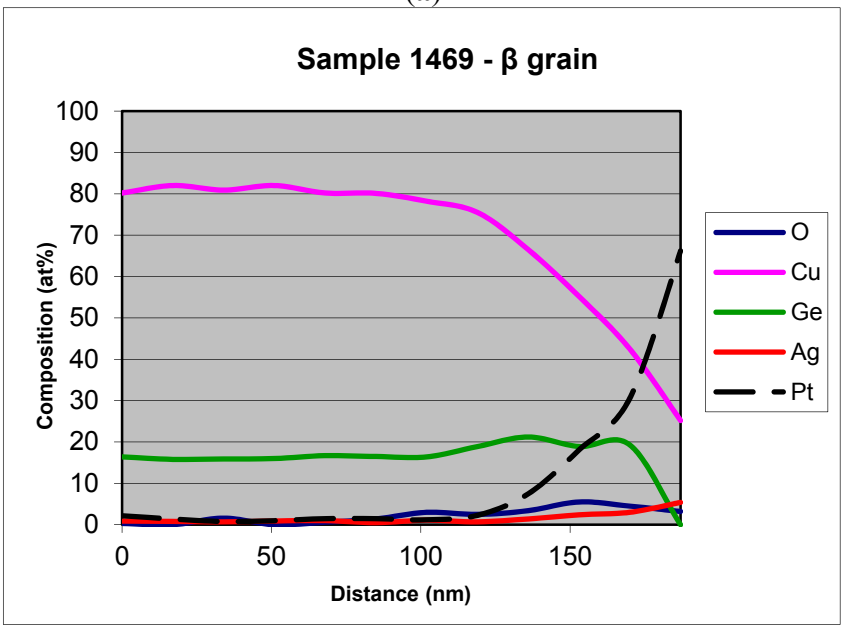

(**b**)

Figure 2. EDS profile distribution of the elements for (**a**) α-phase and (**b**) β-phase of sample 1469.

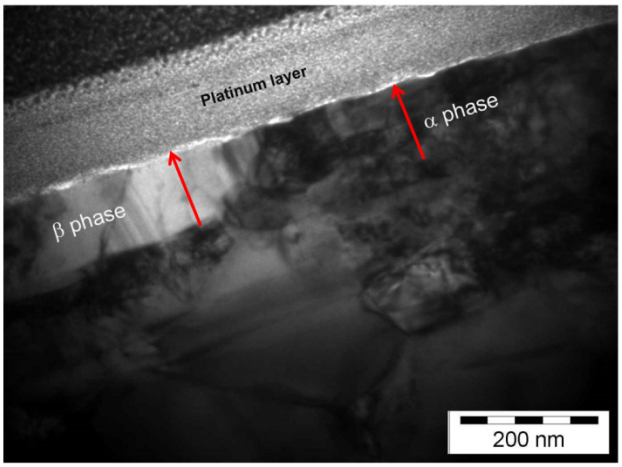

Figure 3. TEM micrograph (120 kV) showing the oxide layer for sample 1469.

Table 1 shows XPS data relative to Ag, Cu, and Ge peaks for all samples. It was found that silver is present only in its metallic state; Cu is present as Cu, CuO, and Cu_2O (it was not possible to separate the peaks of Cu and Cu_2O), while Ge is present in both metallic (Ge) and oxidized (GeO_2) state.

Data reported in Table 1 show that the heat treatment favors the surface concentration of Cu and Ge; this is probably due to the diffusion of germanium (and to a lesser extent, of copper) from the deeper zones of the bulk towards the surface. This diffusion balanced the amount of Ge and Cu that had reacted with oxygen and was removed from the alloy lattice following the oxidation process. It also seems that the heating treatment favors the oxidation of Ge rather than Cu. In sample 1468, treated at 100 °C, the percentage of oxidized germanium is higher by 5% with respect to the non-heated sample; if the heating is prolonged, as for sample 1469, all the Ge is oxidized. Sample 1470, treated at 200 °C, shows again a little metallic Ge, suggesting that the surface oxide may be fragile and may have cracked, thus exposing part of the underneath metallic phase: this is also confirmed by SEM and AFM images.

Table 1. XPS data showing the wt. percentage of each element for all the samples.

Sample	wt% Ag	wt% Cu	wt% Ge	wt% Cu(0) + Cu_2O	wt% CuO	wt% Ge(0)	wt% GeO_2
1467	78.5	19.3	2.2	68.5	31.5	34.4	65.6
1468	78.1	19.2	2.7	74.3	25.7	29.3	70.7
1469	73.9	22.3	3.8	78.8	21.2	0	100
1470	62.6	29.8	7.6	87.5	12.5	19.2	80.8

In Figure 3a TEM micrograph with the detail of sample 1469 is reported showing the two main phases and the thin oxide layer (the thin white line between the alloy and the protective platinum layer). From such images it was possible, for all samples, to measure the thickness of the oxide layer.

A histogram with the estimated average thickness of the oxide layers is shown in Figure 4: it is clearly visible that a higher temperature is responsible for the increase of the total oxide layer, rising from 4 ± 1 nm for sample 1467 (no heat treatment) to 19 ± 5 nm for sample 1470 (200 °C).

For all samples (1470 excluded) it was shown that the oxide layer is thicker in the β-phase than in the α-phase. Only in sample 1469 is germanium oxide thickness uniformly distributed between the two main phases. For sample 1467, which did not undergo any heating treatment, no protective oxide layer was observed in the main phase. Also, in sample 1470 the oxide is about to crack, revealing it to be porous

and fragile, as shown in Figure 5a; the porous oxide structure is clearly visible. For comparison, Figure 5b shows an image of sample 1469 whose protective oxide layer is revealed to be thin and dense. Figure 5c shows a section of sample 1470 in which the cracks in the oxide layer are evidenced in circles.

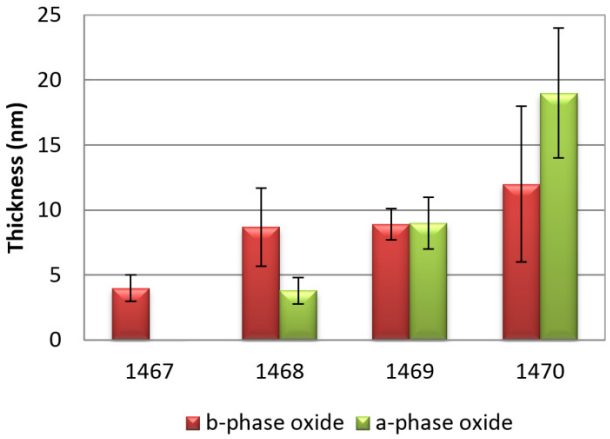

Figure 4. Histogram of the oxide thickness for all samples.

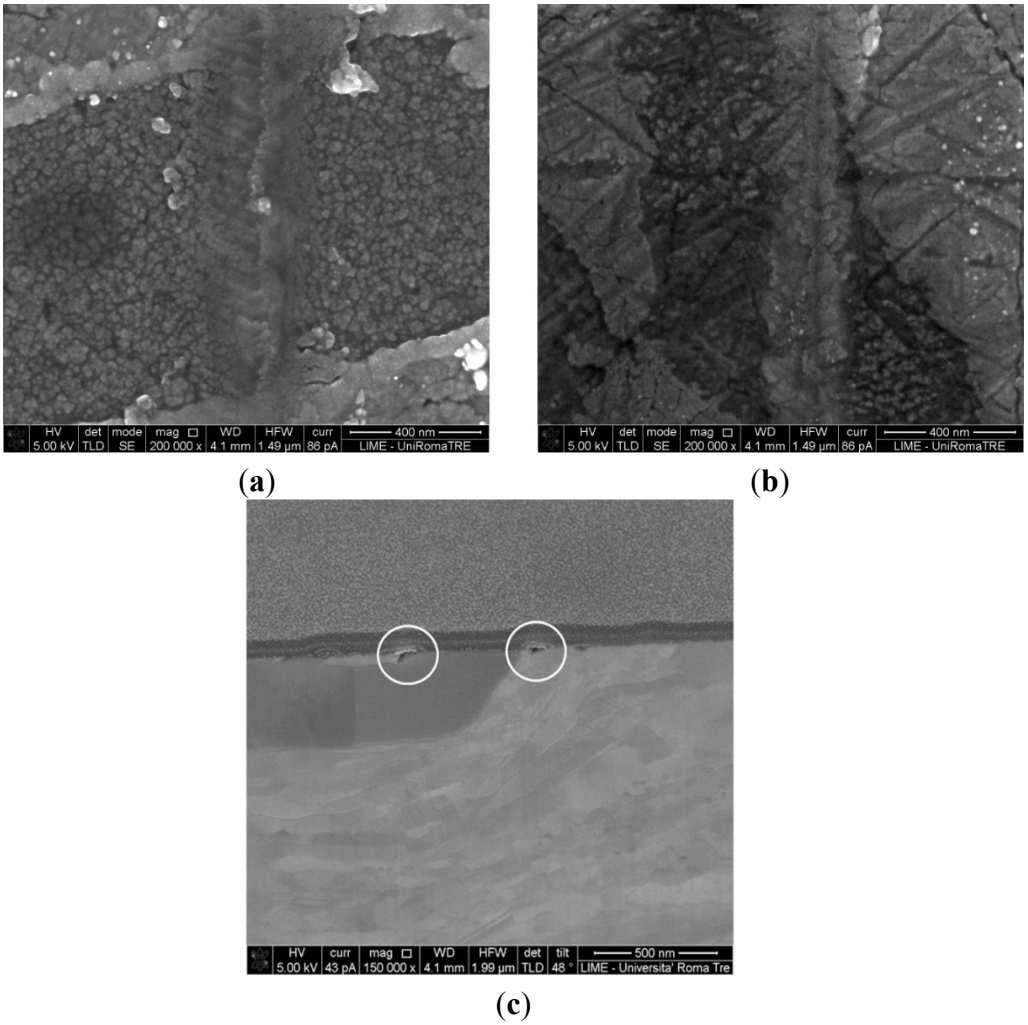

Figure 5. (**a**) SEM image of the 1470 oxide layer showing a porous structure; (**b**) SEM image of the 1469 sample, showing a thin and dense oxide film; (**c**) Section of sample 1470 showing the film cracks in the points circled.

A thicker oxide layer, in conjunction with a more porous and more inhomogeneous surface morphology, could lead to a more brittle behavior of the oxide layer itself, as in the case of sample 1470.

AFM images confirm that all samples have the typical two-phase structure, with an Ag-rich matrix (α), and clusters of a β, Cu-rich, phase. In all samples the Cu-rich phase is made of clusters slightly higher than the matrix: this is due to the higher hardness of the β-phase oxide, so that during polishing a minor quantity of material is removed. As we already know from EDS, it is in this second phase that most of the germanium is alloyed.

Figure 6 shows the different morphology, for sample 1468, passivated at 100 °C, for the two different phases. The Cu-rich phase is characterized by roundly shaped grains (about 40–60 nm in diameter) which tend to agglomerate in height to form bigger structures (130–180 nm), while the Ag-rich phase is constituted by grains of 30–50 nm in diameter which tend to agglomerate in a longitudinal direction.

A similar trend is confirmed for all samples, not shown here for brevity. The second phase also show mean roughness values that are slightly higher than those measured for the Ag-rich matrix, as shown in Table 2. The mean roughness reported here is measured according to the ISO 4287 standard [23], and it is relative to a 1 × 1 μm area, since the inclusions of the β-phase are very small.

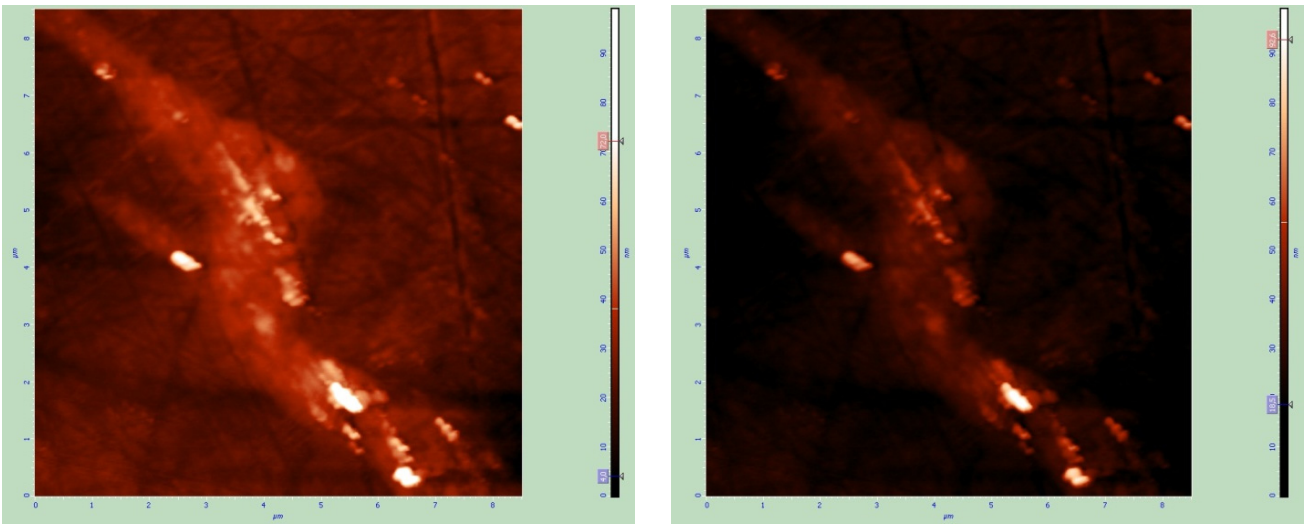

(**a**) (**b**)

Figure 6. AFM images (8 μm × 8 μm) of sample 1468. The same image is shown with two different values of color contrast: (**a**) A brighter contrast was used to evidence the microstructure of α-phase, while (**b**) a darker contrast is used for β-phase.

Table 2 also shows, for all samples, the value of the mean roughness, measured on the maximum area possible to scan with AFM.

Due to a non-planarity of some samples and to the impossibility to perform any surface cleaning prior to the data acquisition with AFM—to avoid altering the result—the maximum scan area that was possible to acquire without any artefacts or contamination in the imaging, was 50 μm × 50 μm. The reported values refer to an average of five different areas for each sample. It is clear, from the data in Table 2, that an increase of the passivation temperature induces an increase of the mean roughness, rising from 3.7 nm for the sample with no heat treatment to 4.4 nm (average) for the samples passivated at 100 °C, to 7.1 nm for the sample heated at 200 °C. The increase of the mean roughness is in agreement with the

presence of a thicker oxide layer in the samples treated at higher temperature, since it was observed that the grains of the β phase tend to agglomerate to form higher, and rougher, structures.

Table 2. Average roughness parameters calculated on a 50 μm × 50 μm scan area for all the samples.

Sample	Heating	R_a [nm]
1467	r.t.	3.7
1468	100 °C	4.2
1469	100 °C	4.6
1470	200 °C	7.1

AFM also confirmed that sample 1470 has a fragile surface oxide that tends to exfoliate, as shown in Figure 7.

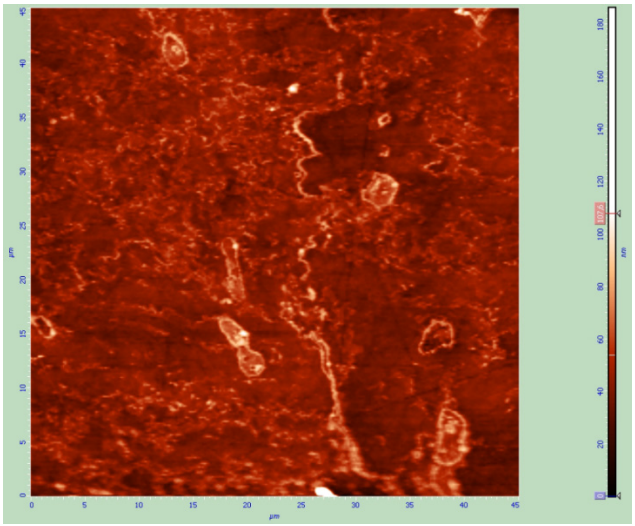

Figure 7. AFM image (45 μm × 45 μm) of sample 1470.

3.2. Micromechanical Characterization

Through nanoindentation hardness and elastic modulus both the main different phases were evaluated for each sample. Figure 8 shows the comparison between the modulus and hardness of the two main phases for all samples (error bars are not shown for clarity).

The results show that for all samples, the bulk properties are almost the same, as shown in the graphics above, at the higher values of displacement into surface. Furthermore, for all samples, indentation on the Cu-rich grains shows higher elastic modulus and higher hardness, in comparison with the Ag-rich matrix: the value of the hardness on the Ag-rich phase, at a displacement value of 40 nm, goes from about 3.17 to 4.04 GPa, while, at the same value of displacement, the hardness measured on the Cu-rich phase ranges from 4.53 to 8.09 GPa. Also the modulus shows the same behavior ranging from 86.38 to 106.78 on the α-phase while it goes from 107.91 to 138.22 GPa in the β-phase.

An increase of both hardness and modulus is observed for the Ag-rich phase at penetration depth lower than 50 nm: this is likely due to a pileup effect which usually involves an overestimation of the elastic modulus at penetration depths lower than 50 nm for soft metals with a surface hardened layer (due to the forming process) [15].

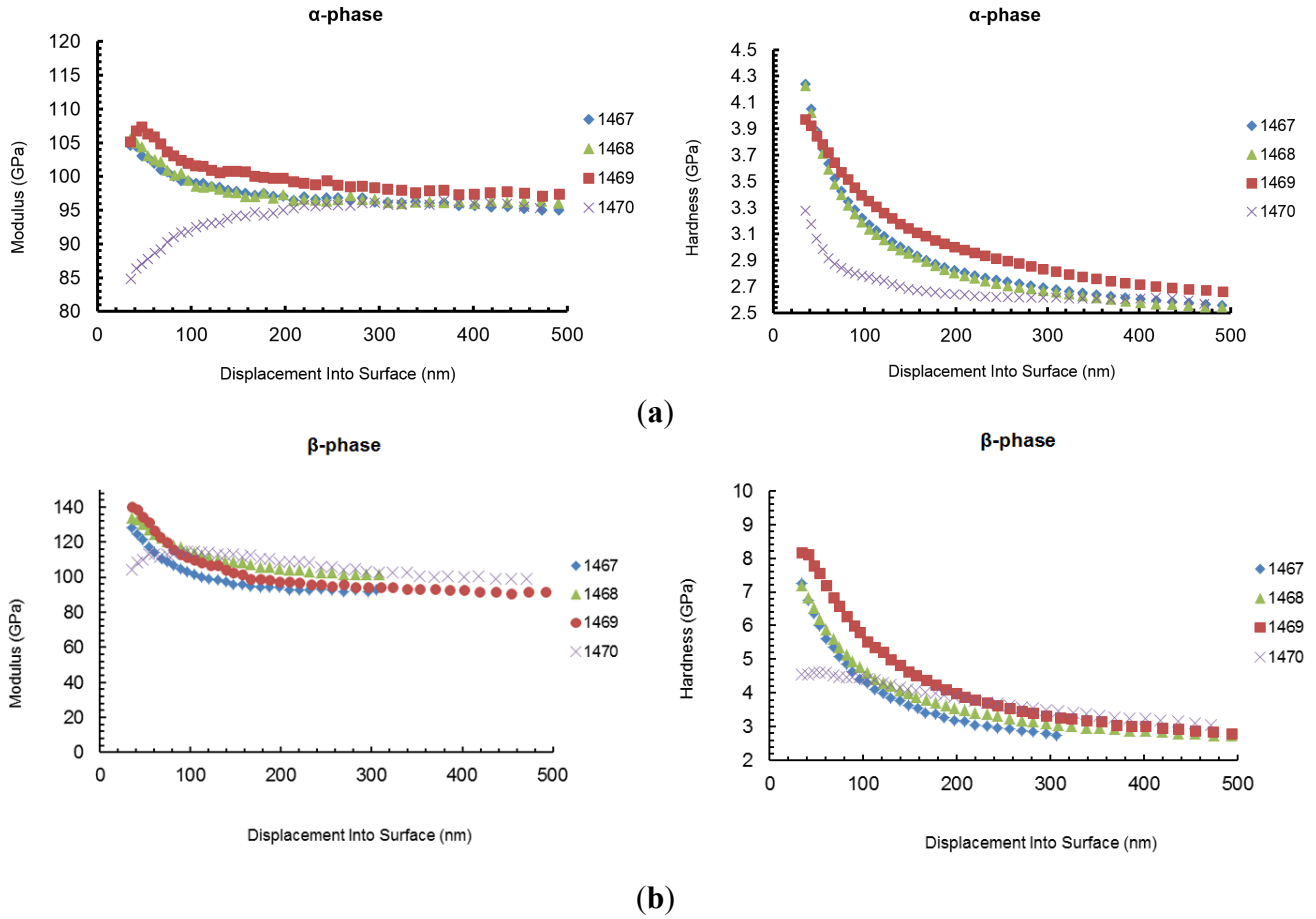

Figure 8. Comparison between the modulus and hardness of the (**a**) α phase and (**b**) β phase for all samples.

Sample 1470 shows a completely different mechanical behavior at penetration depths lower than 100 nm. In particular, a significantly lower hardness is measured, in comparison with the other samples, and a marked reduction of the elastic modulus is observed for penetration depths lower than 60 nm.

Two different explanations can be proposed for this effects: the presence of a brittle surface oxide layer (as seen with TEM and AFM) or a partial recrystallization (or at least stress relieving) in correspondence with the surface hardened layer; in fact a modification of the surface residual stress could even cause a decrease of the apparent measured elastic modulus: this effect is obviously not real (modulus is not affected by residual stress), but it is observed in nanoindentation testing because a variation of the surface residual stress usually involves a modification of the contact area during indentation.

Nanoscratching was performed by means of a Berkovich nanoindenter with the aim to gain information on the wear resistance of the samples. Displacement into surface *vs.* scratch distance curves were also performed, although not shown here for brevity. The results showed that the Cu-rich phases are more resistant to scratch, as a consequence of their higher hardness; this result was confirmed after SEM imaging of the scratches: the width of the scratch is significantly reduced in correspondence with the Cu-rich grains, as shown in Figure 9, as examples, for samples 1467 and 1468. In Figure 10 the histogram of the friction coefficient for all the samples is reported. It is possible to notice that the friction coefficient greatly decreases for samples treated at 100 °C (friction coeff. = 0.236 for sample 1468 and 0.164 for sample 1469), with respect to the room temperature sample (friction coeff. = 0.653). This

suggests that the oxide layer that forms at this temperature might act as a solid state lubricant, greatly reducing the friction coefficient. A reduction of the friction coefficient directly involves a reduction of the surface contact stress during sliding contact, thus enhancing the scratch and wear resistance of the component. Also, the higher values of surface roughness evidenced by AFM for sample 1470 could give rise to significantly higher values of surface contact stresses during nanoscratch tests [18].

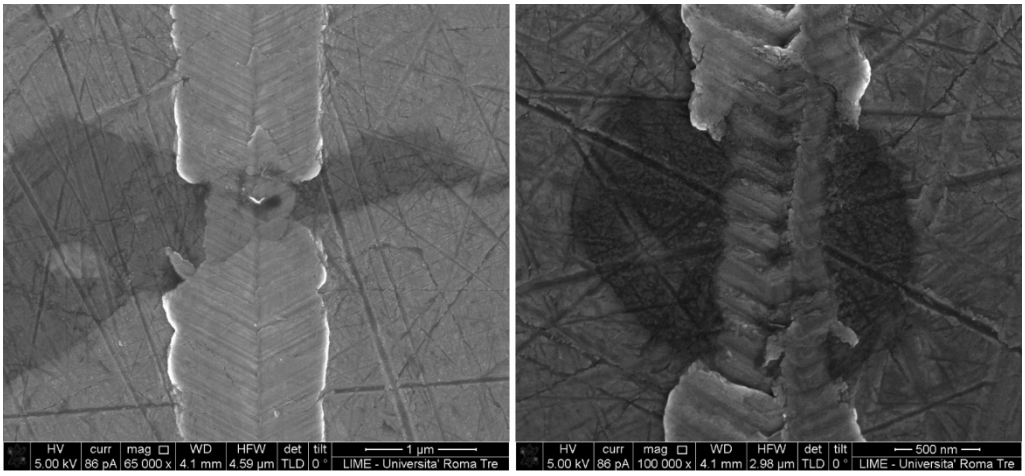

(**a**) (**b**)

Figure 9. SEM micrographs of the scratches indented on samples (**a**) 1467 and (**b**) 1468.

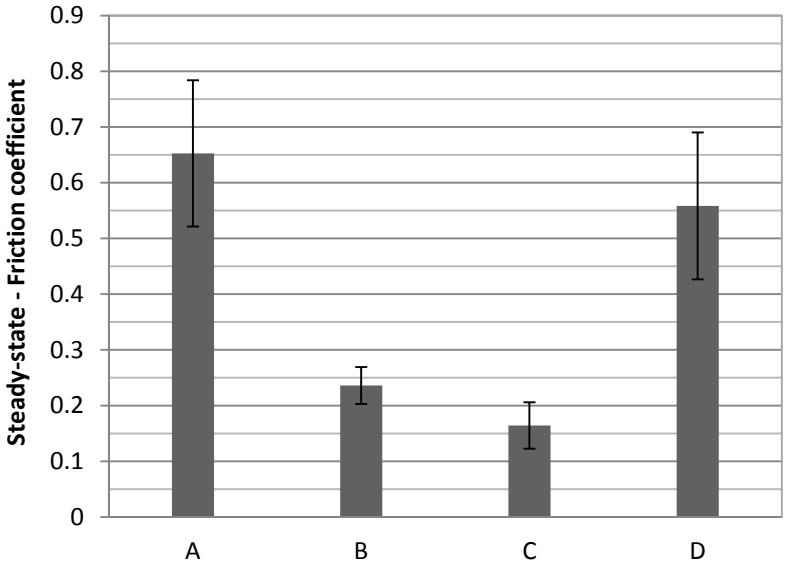

Figure 10. Values of the friction coefficient for all samples. A: 1467; B: 1468; C: 1469; D: 1470.

We can conclude that the addition of germanium to Sterling silver, and an opportune passivation treatment, not only improves its tarnishing and fire stain resistance, reducing the frequency of the re-polishing and increasing the time between one re-polishing treatment and the subsequent one, but it also increases the wear resistance of the alloy. This is particularly desirable since re-polishing of tarnished silver often produces wear and scratches causing the material to lose its pristine appearance.

While increasing passivation time produces a better friction coefficient, a different behavior occurs if the temperature is too high. For the sample treated at 200 °C the value of the friction coefficient rises up almost to the value of the non-treated sample (friction coeff. = 0.558). Once again this is in agreement with the formation of a brittle oxide that cracks up so that the lubrication effect between the probe and the material is lost.

3.3. Further TEM Characterization

To have a further insight on the anomalous behavior of sample 1470, SAED analysis was performed, on this sample and the results were compared with sample 1469.

The electron beam of TEM was moved along a line starting from the "bulk" material and proceeding towards the platinum protective layer; then the areas of the sample in which the diffraction pattern changed were studied. If a change in the spots pattern takes place, then a new crystalline phase is found. If the spots disappear, then an amorphous phase is encountered.

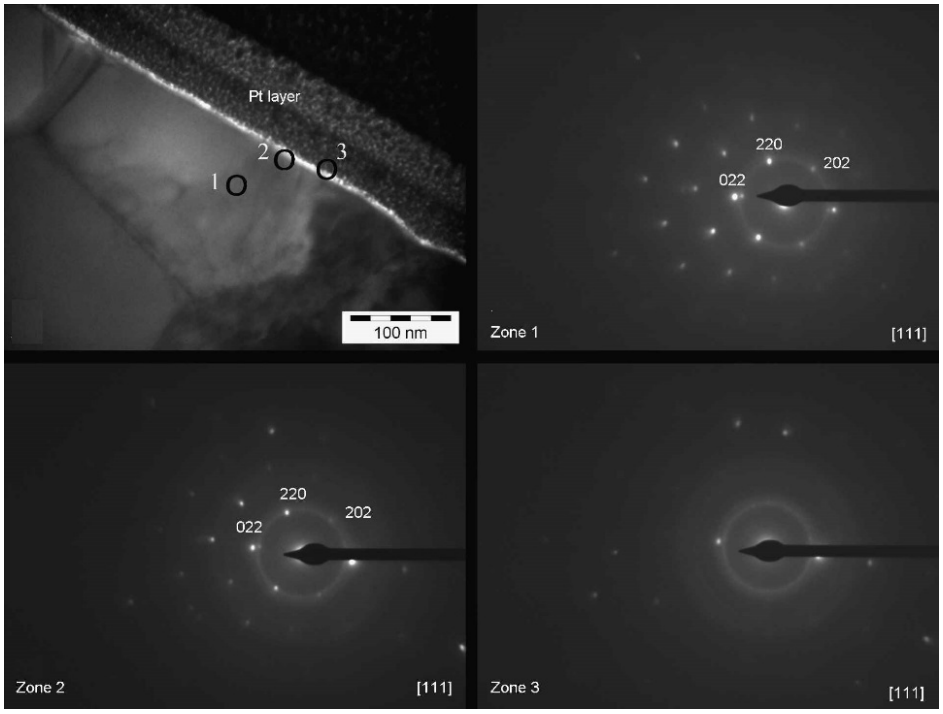

Figure 11. Selected area electron diffraction (SAED) analysis of sample 1469, performed with TEM (120 kV, camera length 470 mm). The circles mark the zones of the diffraction patterns.

Figure 11 shows the SAED results for sample 1469. The images were acquired in three areas: inside the β-phase (zone 1), inside the oxide layer, closer to the alloy (zone 2) and inside the oxide layer, closer to the platinum protective layer (zone 3). Since there is no change in the position of the spots, but only a disappearing of the spots, then no intermediate crystallographic structure between the crystalline cell of β-phase (zone 1) and the amorphous structure of platinum layer is present. Thus, although the oxide layer is extremely thin for this kind of analysis, we can conclude that the structure of the oxide is most likely amorphous, or at least amorphous to a certain degree.

Figure 12 shows the analysis for sample 1470. In this case the analysis was performed in four different areas comprising the β-phase (zone 1), the oxide layer closer to the alloy (zone 2), the oxide layer closer to the platinum protective layer (zone 3) and the platinum layer itself (zone 4).

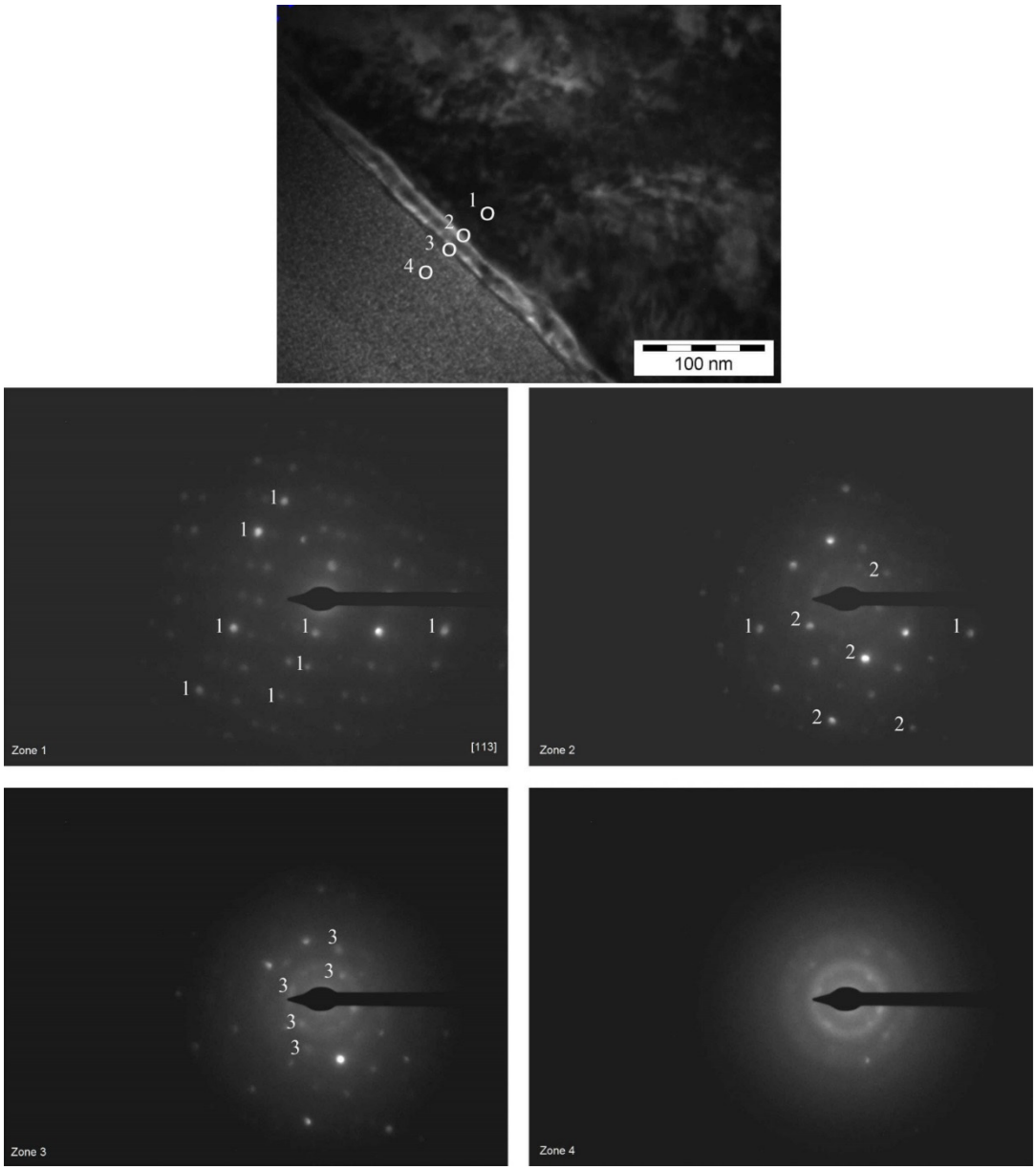

Figure 12. SAED analysis of sample 1470, performed with TEM (120 kV, camera length 470 mm). The circles mark the zones of the diffraction patterns.

A change in the position of the spots is evidenced from the comparison between the four diffraction patterns. The spots marked with (1) in zone 1 tend to disappear while progressing along the path of analysis; however, some new spots appear, those marked with (2). Such patterns clearly show that there is an intermediate crystallographic structure between the cell of β-phase (zone 1) and the structure of the platinum layer (zone 4). Then, in zone 3 a third series of spots appears, which suggests that in this case part of the platinum is crystalline as well. Finally, as shown in zone 4, most of the spots disappear, leaving only the ones that appeared last (crystalline platinum mixed with amorphous platinum; platinum

can be crystalline or amorphous depending on its electronic or ionic nature). We can easily conclude that, in this case, the structure of the oxide layer is crystalline.

The crystallinity of the oxide layer on sample 1470 gives a further explanation of its brittleness, thus confirming the results obtained with AFM and SEM, and of the increase of the friction coefficient observed with the nanoscratching test.

3.4. Tarnishing Test

Figure 13 shows samples 1468 and 1469 after the thioacetamide (TAA) corrosion test, together with a standard Sterling silver sample. As shown, sample 1469 has the best performance against tarnishing: the variation of luminance (ΔL) is 3.5 compared to 10.2 for sample 1468 and 26.7 for the standard Sterling sample. Also the variation of color, ΔE (as defined in [20]), is smaller for sample 1469 (ΔE = 9.0) than sample 1468 (ΔE = 24.3) and standard Sterling (ΔE = 40.6). We can conclude that a passivation time of 16 h not only increases the mechanical properties of the material, but also its tarnishing resistance is greatly improved.

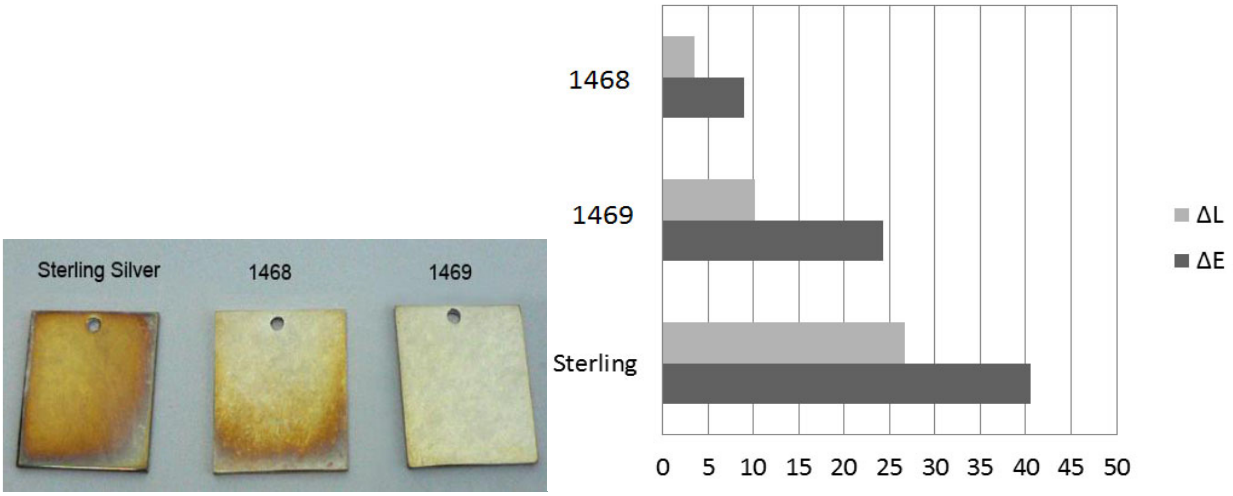

Figure 13. Colorimetric measurement of the samples passivated at 100 °C compared to a standard Sterling silver, after the TAA corrosion test. The graph shows the variation of lightness (ΔL) and color coordinates (ΔE) for each sample after the test.

3.5. General Discussion

All samples showed a typical two phase structure, with a Cu rich second phase included in an Ag rich matrix. Sample 1467 was not heat treated and the β-phase inclusions present a lamellae spacing due to the lamination of the sample. The heat treatment relaxes the distribution of the inclusions which appear more randomly dispersed (Figure 1).

A thin oxide layers forms in all heated samples, and it appears that the annealing improves the concentration of germanium on the surface. Preferential oxidation of germanium rather than copper is evident in sample 1469 with respect to sample 1468 and 1467.

Samples 1467, 1468, and 1469 bulk properties are almost the same and their Cu-rich grains show higher elastic modulus and hardness, in comparison with the Ag-rich matrix. Sample 1470 shows a

different mechanical behavior since a significantly lower hardness is measured, and a marked reduction of the elastic modulus is observed: this has been related to the formation of a brittle oxide layer.

A passivation temperature of 100 °C and a time of 16 h are the best experimental conditions to produce a wear resistant, uniformly distributed oxide layer. A sample prepared under such parameters also proved to have the higher tarnish resistance.

Sample 1470 was treated at a significant higher temperature than samples 1468 and 1469 but for less time. In this case, however, the resulting material performed poorly, as it was covered by a thick, brittle oxide that cracked and did not provide the tarnishing protection required.

4. Conclusions

Samples of a ternary Ag-Cu-Ge alloy were characterized from structural, morphological, and a mechanical point of view. It has been found that:

1. Samples are composed of two phases, with copper rich clusters dispersed in a silver rich matrix. This is consistent with a slow, equilibrium cooling.
2. The majority of germanium is alloyed in the Cu-rich β-phase.
3. Only germanium and copper are present in the oxidized state, the latter being present in two different oxides: CuO and Cu_2O; germanium is found as GeO_2 and in its metallic state, while silver is all metallic.
4. The thickness of the oxide layer increases with the increase of passivation temperature; an increase of passivation time produces oxide layers whose thickness is uniform in the two phases.
5. The surface roughness of the samples is higher in the β-phase, than in the α one. Consistently with the previous point, an increase of passivation temperature induces an increase of surface roughness.
6. The friction coefficient is significantly reduced for samples treated at 100 °C, due to the presence of a thin and dense oxide layer on the Ag-rich phase that acts as a solid state lubricant; the addition of germanium to Sterling silver, followed by an adequate heat treatment, not only improves its tarnishing and fire stain resistance, but also increases the wear and scratch resistance of the alloy.
7. The sample passivated at the highest temperature is covered with a thicker, brittle, and porous oxide layer: this causes an increase in the friction coefficient and may be the cause of a decrease in the tarnish resistance properties; thus an increase in the heating temperature above a certain limit produces a poor quality material and is to be avoided.

Acknowledgments

Authors would like to acknowledge Chiara Battocchio for technical assistance during XPS analyses. All other characterization activity was performed at the "Interdepartmental Laboratory of Electron Microscopy" of "Roma TRE" University, Rome, Italy (http://www.lime.uniroma3.it).

Author Contributions

Edoardo Bemporad, Marco Sebastiani and Antonio Cusma conceived and designed the experiments; Marco Sebastiani performed the Nanoindentation and Nanoscratching experiments; Daniele deFelicis performed the SEM, EDS, FIB and TEM-SAED experiments; Antonio Cusma performed the AFM experiments; Andrea Basso performed the corrosion and colorimetric tests; all authors analyzed the data; Andrea Basso contributed materials; Antonio Cusma wrote the paper.

Conflicts of Interest

The authors declare no conflict of interest.

References

1. Johns, P.G. Alloy with Boron as Grain Refiner for Joining Metals by Non-Filler Welding Techniques, e.g., Diffusion, at Temperatures below the Solidus Temperature of the Materials Being Joined; Jewelry, Silverware, Electric Contacts, and Aerospace. US Patent 6,168,071 B1, 2 January 2001.
2. Johns, P.G. Silver Ternary Alloy. US Patent 2007/009375 A1, 11 January 2007.
3. Johns, P.G.; Harrison, C.E. Enhancing Silver Tarnish-Resistance. US Patent 2007/0039665 A1, 22 February 2007.
4. Federal Trade Commission. Guides for the metallic watch band industry and guides for the jewelry industry. *Fed. Regist.* **1996**, *61*, 27178–27222.
5. Nisaratanaporn, E.; Wongriruksa, S.; Pongsukitwat, S.; Lothongkum, G. Study on the microstructure, mechanical properties, tarnish and corrosion resistance of sterling silver alloyed with manganese. *Mater. Sci. Eng. A* **2007**, *445–446*, 663–668.
6. Gardam, G.E. Sterling silver containing aluminium. *Metallurgia* **1953**, *47*, 29–33.
7. Reti, A.M. Understanding Sterling Silver. In Proceedings of the 11th Santa Fe Symposium on Jewellery Manifacturing Technology, Albuquerque, NM, USA, 18–21 May1997; p. 353.
8. McCloskey, J.C.; Welch, P.R.; Aithal, S. Silicon microsegregation in 14K yellow gold jewelry alloys. *Gold Technol.* **2000**, *30*, 4–7.
9. Johns, P. Fire Stain Resistant Silver Alloys. In Proceedings of the 11th Santa Fe Symposium on Jewellery Manifacturing Technology, Albuquerque, NM, USA, 18–21 May 1997; pp. 38–42.
10. Dawson, G.; Grice, S.; Nyce, A. A Study Comparing Commercially Available Tarnish-Resistant Sterling Silver Alloys with a Traditional Sterling Silver. In Proceedings of the 20th Santa Fe Symposium on Jewellery Manifacturing Technology, Nashville, TN, USA, 10–13 September 2006; pp. 121–154.
11. Gayler, M.L.V.; Carrington, W.E. Metallographic study of the precipitation of copper from a silver-rich silver-copper alloy. *J. Inst. Met.* **1947**, *73*, 625–639.
12. Scharfenberger, W.; Schmitt, G.; Borchers, H. Uber die kinetic der diskontinuierlichen ausscheidung der silberlegierung mit 7.5 gew% Cu. *Z. Metallk.* **1972**, *63*, 553–560. (In German)
13. Youssef, S.B. Resistometric study of Ag–8 at% Cu alloy aged in the temperature-range 0.4–0.65 T_m. *Physica B* **1996**, *228*, 337–341.

14. Colombo, S.; Battaini, P.; Airoldi, G. Precipitation kinetics in Ag–7.5 wt.% Cu alloy studied by isothermal DSC and electrical-resistance measurements. *J. Alloys Compd.* **2007**, *437*, 107–112.
15. Oliver, W.C.; Pharr, G.M. Measurement of hardness and elastic modulus by instrumented indentation: Advances in understanding and refinements to methodology. *J. Mater. Res.* **2004**, *19*, 3–20.
16. Bolshakov, A.; Pharr, G.M. Influences of pileup on the measurement of mechanical properties by load and depth sensing indentation techniques. *J. Mater. Res.* **1998**, *13*, 1049–1058.
17. Schuh, C.A.; Nieh, T.G.; Yamasaki, T. Hall-Petch breakdown manifested in the abrasive wear resistance of nanocrystalline nickel. *Scr. Mater.* **2002**, *46*, 735–740.
18. Menezes, P.L.; Kishore, S.; Kailas, V. Studies on friction and transfer layer: role of surface texture. *Tribol. Lett.* **2006**, *24*, 265–273.
19. *ISO 4538 Metallic Coatings—Thioacetamide Corrosion Test (TAA Test)*; International Standard Organization: Geneva, Switzerland, 1978.
20. *Industrial Colour-Difference Evaluation*; Technical report 116/1995 ed; Commission Internationale de I'Eclairage Central Bureau: Vienna, Austria, 1995.
21. Sampath Kumar, T.S.; Mallya, R.M.; Hedge, M.S. Surface segregation and oxidation studies on Cu-Ni-Sn and Ag-Cu-Ge ternary alloys. *Appl. Surf. Sci.* **1989**, *35*, 63–75.
22. Wang, N.; Wei, B. Rapid crystallization and growth mechanisms of highly undercooled Ag–Cu–Ge ternary alloy. *J. Cryst. Growth* **2003**, *247*, 576–586.
23. *ISO 4287 Geometrical Product Specifications (GPS)—Surface texture: Profile method—Terms, Definitions and Surface Texture Parameters*; International Standard Organization: Geneva, Switzerland, 2009.